Spectral and spread-spectral teleportation

Travis S. Humble*

Computer Science and Mathematics Division, Oak Ridge National Laboratory, Oak Ridge, Tennessee, 37831-6015 USA

(Received 8 March 2010; revised manuscript received 23 April 2010; published 25 June 2010)

We report how quantum information encoded into the spectral degree of freedom of a single-photon state may be teleported using a finite spectrally entangled biphoton state. We further demonstrate how the bandwidth of the teleported wave form can be controllably and coherently dilated using a spread-spectral variant of teleportation. We calculate analytical expressions for the fidelities of spectral and spread-spectral teleportation when complex-valued Gaussian states are transferred using a proposed experimental approach. Finally, we discuss the utility of these techniques for integrating broad-bandwidth photonic qubits with narrow-bandwidth receivers in quantum communication systems.

DOI: 10.1103/PhysRevA.81.062339 PACS number(s): 03.67.Hk, 03.67.Mn, 42.50.Dv

I. INTRODUCTION

As a fundamental means of quantum communication, quantum teleportation has been realized in various theoretical and experimental forms with each form adopting a specific physical system to encode the underlying quantum information [1]. Quantum optical systems have proven particularly useful for realizing many of these different variants. For example, protocols encoding quantum information into continuous variables like the field quadratures [2,3] or temporal modes [4], as well as discrete variables like the polarization [5,6], have already been demonstrated, while schemes using the transverse-spatial degrees of freedom, including orbital angular momentum, have been proposed [7]. As a complement to these prior formulations, we present and analyze a method for teleporting quantum information encoded into the spectral state of a single photon.

Spectral teleportation uses entanglement in the joint spectral amplitude of a biphoton state to mediate the transfer of a single-photon spectral amplitude. Spectral entanglement arises naturally, for example, in the biphoton states generated by spontaneous parametric down-conversion (SPDC), where conservation of energy and phase-matching constraints specify preparation of the joint spectral amplitude. Indeed, it was soon after the initial proposal for quantum teleportation that Molotkov introduced teleportation of a single-photon spectral state based on the Einstein-Podolsky-Rosen (EPR)-correlated pairs generated through cw-pumped SPDC [8,9]. In particular, Molotkov showed that for the case of infinite spectral entanglement and bandwidth, biphoton up-conversion would lead to remote preparation of a single-photon spectral wave packet in a manner that closely resembles other continuous-variable (CV)-based protocols [2].

Broader insight into the behavior of spectral teleportation with respect to the spectral entanglement or the spectral bandwidths requires the consideration of imperfect EPR correlations. Such considerations arise naturally with the use of pulsed SPDC sources, that is, SPDC pumped by broad bandwidth pulses, where the amount of spectral entanglement generated varies strongly with source design and, especially, the underlying phase-matching function [10]. As pulsed SPDC sources provide a means of timing the interference or overlap of photons from different sources, the understanding of finite entanglement and bandwidth on the fidelity of spectral teleportation would seem necessary. Motivated by these considerations, we investigate the role of finite spectral entanglement and bandwidth on the spectral teleportation fidelity, and we assess the potential for high-fidelity spectral teleportation using available down-conversion sources.

We also report that spectral teleportation can be used to coherently modulate the bandwidth of a teleported wave form. Specifically, this spread-spectral variant of teleportation enables the single-photon spectral state to be coherently dilated with respect to the probability amplitude. While spectral and spread-spectral teleportation share common elements, we show that the underlying distinction is the requirement placed on the marginal bandwidth ratio of the joint spectral amplitude mediating the process. We subsequently analyze the fidelity of spread-spectral teleportation with respect to both finite entanglement and bandwidth. Ultimately, we expect that spread-spectral teleportation may prove useful for interfacing broadband photonic qubits with narrowband quantum receivers, for example, quantum memory devices. This capability complements efforts to coherently modulate the single-photon carrier frequency based on up-conversion, for example, to shift from IR to visible wavelengths in order to improve detection efficiency [11–14].

The theory for spectral teleportation of a single-photon state is presented in Sec. II and analyzed in Sec. III using complex-valued Gaussian amplitudes to derive the spectral teleportation fidelity. Similarly, spread-spectral teleportation is described in Sec. IV with the spread-spectral teleportation fidelity for Gaussian states presented in Sec. V. The potential implications of spectral and spread-spectral teleportation for quantum communication are discussed in Sec. VI while final conclusions are drawn in Sec. VII.

II. SPECTRAL TELEPORTATON

Consider a single, spectrally multimode photon described by the pure state

$$|\psi_1\rangle = \int \alpha(\omega)|\omega_1\rangle d\omega\,, \tag{1}$$

*humblets@ornl.gov

where $\alpha(\omega)$ is the normalized spectral probability amplitude and $|\omega_1\rangle$ is the spectral eigenstate of photon 1 at frequency ω. The state (1) may be generated, for example, using either on-demand single-photon sources or heralding photon-pair sources. Let the transverse-spatial and polarization degrees of freedom be prepared in single-mode, pure states, for example, using spatial filters and polarizing beamsplitters, respectively.

Spectral teleportation transfers the amplitude $\alpha(\omega)$ of photon 1 to a remote photon 3, where the latter is initially prepared with photon 2 in the normalized biphoton state

$$|\varphi_{23}\rangle = \int d\omega \int d\omega' f(\omega,\omega')|\omega_2,\omega_3'\rangle \tag{2}$$

and the joint spectral probability amplitude $f(\omega,\omega')$ determines the spectral entanglement of the pair. The Schmidt decomposition of the joint spectral amplitude is [15]

$$f(\omega,\omega') = \sum_{n=0}^{\infty} \lambda_n^{1/2} u_n(\omega) v_n(\omega'), \tag{3}$$

where λ_n is the nth Schmidt coefficient and normalization implies

$$\sum_{n=0}^{\infty} \lambda_n = 1. \tag{4}$$

The nth pair of Schmidt modes $u_n(\omega)$ and $v_n(\omega')$ belongs to a biorthogonal set that spans the joint spectral Hilbert space. The biphoton state (2) is spectrally entangled when there exists more than one term in the summation of Eq. (3). Specifically, when the joint amplitude is inseparable, that is,

$$f(\omega,\omega') \neq u_0(\omega) v_0(\omega'), \tag{5}$$

then the photon pair is spectrally entangled. A convenient measure for quantifying the spectral entanglement is the Schmidt number [15]

$$K \equiv \sum_{n=0}^{\infty} \lambda_n \Big/ \sum_{n=0}^{\infty} \lambda_n^2, \tag{6}$$

which grows from unity as the number of nonzero Schmidt coefficients increases.[1] Experimentally, the presence of spectral entanglement may be inferred from the reduced visibility of the Hong-Ou-Mandel dip when using independent sources [10,16–18], while measurements of joint spectral amplitudes generated by current SPDC sources yield spectral Schmidt numbers as large as ~600 with the potential to be much larger [18–21].

Spectral teleportation is implemented by up-converting photons 1 and 2 into a higher-frequency photon 4 [8,9]. The latter is subsequently subjected to a spectrally resolved measurement that effectively transforms the state of photon 3. Specifically, consider the case that photons 1 and 2 undergo sum-frequency generation (SFG) in a nonlinear optical medium to generate photon 4. This form of up-conversion requires phase matching of photons 1 and 2 over the relevant bandwidth, with the overall conversion efficiency determined by the second-order nonlinear susceptibility tensor $\chi^{(2)}_{\mathrm{SFG}}$. Assuming perfect phase matching across the bandwidths of photons 1 and 2, and taking $\chi^{(2)}_{\mathrm{SFG}}$ as constant, the up-converted photon 4 has a mean frequency $\bar{\omega}_4 = \bar{\omega}_1 + \bar{\omega}_2$, where $\bar{\omega}_1$ and $\bar{\omega}_2$ are the mean frequencies of photons 1 and 2, respectively. Following up-conversion, the joint state of photons 3 and 4 is then given by

$$|\xi_{34}\rangle = c \int d\omega \int d\omega' \int d\omega'' \alpha(\omega) \times f(\omega',\omega'')|\omega_3'',(\omega+\omega')_4\rangle, \tag{7}$$

where c is the normalization factor.

As a result of the spectral entanglement in Eq. (7), a spectral measurement of photon 4 transforms the state of photon 3. This spectral measurement may be modeled in its simplest form as a projection onto a frequency eigenstate $|\Omega_4\rangle$. That projective measurement prepares photon 3 in the pure state,

$$|\tilde{\psi}_3\rangle = \eta \int d\omega \int d\omega' \alpha(\omega) f(\Omega-\omega,\omega')|\omega_3'\rangle, \tag{8}$$

where the tilde denotes an intermediate result and the normalization factor η, defined by

$$|\eta|^{-2} = \sum_{n=0}^{\infty} \lambda_n |a_n(\Omega)|^2, \tag{9}$$

depends on the measurement outcome Ω via the convolution integral

$$a_n(\Omega) = \int \alpha(\omega)\, u_n(\Omega-\omega) d\omega. \tag{10}$$

The intermediate spectral state (8) may be well understood in the limit that photons 2 and 3 are perfectly entangled in frequency, for example, the case where the joint spectral amplitude approaches the δ distribution

$$f(\omega,\omega') \to \delta(2\bar{\omega}_0 - \omega - \omega'). \tag{11}$$

In this limit, the Schmidt coefficients are identical and the Schmidt number K approaches infinity.[2] This form of the joint spectral amplitude is well-approximated by cw pumping of the SPDC process, where the quantity $2\bar{\omega}_0$ represents the pump frequency, and corresponds to the case first considered by Molotkov [8]. By inserting the approximate joint spectral amplitude of Eq. (11) into Eq. (8), the state of photon 3 after normalization is found to be

$$|\tilde{\psi}_3\rangle = \int d\omega\, \alpha(\omega)|(\omega-\Delta)_3\rangle, \tag{12}$$

where $\Delta = \Omega - 2\bar{\omega}_0$ is a spectral offset due to quantum-mechanical indeterminism inherent to the spectral state of photon 4. The measurement information Δ may be used to locally transform the state of photon 3 defined by Eq. (12) as to

[1] This definition of K accounts for normalization of the joint spectral amplitude, which is conventionally unity but may not be the case [cf. Eq. (11)].

[2] In the limit (11), the bandwidths of photons 1 and 2 are infinite and the spectral state is non-normalizable while the Schmidt modes are represented by any complete set of biorthogonal functions. The case of infinite entanglement with finite bandwidth is considered in Sec. III.

match the state of photon 1 in Eq. (1). For example, using either difference-frequency generation with a pump pulse having frequency Δ [14] or an acousto-optic frequency shifter driven at frequency Δ applies the necessary shift to the spectral state. Thus, in principle, unit spectral teleportation fidelity may be obtained.

The preceding limiting case suggests a protocol for spectral teleportation with an arbitrary joint spectral amplitude. By shifting the spectral state in Eq. (8) an amount Δ, this spectral teleportation protocol prepares the state of photon 3 as

$$|\psi_3\rangle = \eta \int d\omega \int d\omega' \alpha(\omega) f(\Omega-\omega,\omega'-\Delta)|\omega_3'\rangle. \quad (13)$$

The corresponding spectral teleportation fidelity is the squared magnitude overlap of Eq. (13) with Eq. (1) and is given by

$$F = \left|\eta \int d\omega \int d\omega' \alpha(\omega) f(\Omega-\omega,\omega'-\Delta)\alpha(\omega')^*\right|^2. \quad (14)$$

In general, the fidelity (14) depends on the spectral shift Δ, as well as the spectral entanglement carried by the joint spectral amplitude. Moreover, the value of Δ that optimizes the teleportation fidelity depends on the properties of the entangled photon pair including the relative bandwidths and the amount of spectral entanglement. As shown previously, unit fidelity teleportation is achieved in the limit of infinite spectral entanglement, but for the case of finite entanglement, an average spectral teleportation fidelity, $\langle F\rangle$, must be computed with respect to the distribution of possible spectral input states. We return to the averaging procedure after first considering the specific example of Gaussian spectral teleportation.

III. GAUSSIAN SPECTRAL TELEPORTATION

We investigate the behavior of the spectral teleportation fidelity (14) for the case of finite spectral entanglement and finite bandwidths. We consider the case of a spectrally entangled photon pair generated by broad-bandwidth pumping of SPDC. It has been shown previously that the joint spectral amplitude generated by broad-bandwidth SPDC may be expressed as

$$f(\omega,\omega') = A(\omega+\omega')\Phi(\omega,\omega'), \quad (15)$$

where $A(\omega)$ is the pump-pulse spectrum and $\Phi(\omega,\omega')$ is the spectral phase-matching function [10]. The phase-matching function $\Phi(\omega,\omega')$ depends on the birefringence of the crystal and the pump properties. For type-II SPDC in the short-pulse limit, the phase-matching function may be reduced to a one-dimensional Gaussian (cf. the Appendix). When the pump spectrum $A(\omega)$ is also Gaussian, an analytic approximation for the joint spectral amplitude parametrized by three independent quantities is obtained, that is,

$$f(\omega,\omega') = N\exp\left\{-\frac{1}{2}\left[\frac{(\omega-\bar\omega_2)^2}{\gamma_2^2}+\frac{(\omega'-\bar\omega_3)^2}{\gamma_3^2} - \frac{2\rho\,(\omega-\bar\omega_2)(\omega'-\bar\omega_3)}{\gamma_2\gamma_3}\right]\right\}, \quad (16)$$

where $\bar\omega_2$ and $\bar\omega_3$ are the mean frequencies of photons 2 and 3, respectively, σ_2 and σ_3 are the corresponding bandwidths, $\rho \in [-1,1]$ is the linear correlation between photon frequencies, $\gamma_j^2 = \sigma_j^2(1-\rho^2)$ is for convenience, and N is a normalization constant defined by $N^{-2} = \pi\sigma_2\sigma_3\sqrt{1-\rho^2}$. For completeness, these parameters are expressed in terms of experimental conditions in the Appendix.

The Schmidt coefficients of the Gaussian joint amplitude in Eq. (16) are [17]

$$\lambda_n = \operatorname{sech}^2\zeta \tanh^{2n}\zeta, \quad (17)$$

where the angle ζ is defined solely in terms of the linear correlation ρ by

$$\rho = \tanh 2\zeta. \quad (18)$$

Using Eq. (6), the corresponding Schmidt number is found by substitution to be

$$K = \cosh 2\zeta, \quad (19)$$

from which it is apparent that the spectral entanglement measured by K approaches infinity as $|\rho|$ approaches unity. The Schmidt modes for the joint amplitude (16) are Hermite functions over the appropriate bandwidth scales, that is, $u_n(\omega) = h_n^{\gamma_2}(\omega-\bar\omega_2)$ and $v_n(\omega) = h_n^{\gamma_3}(\omega-\bar\omega_3)$ with the nth normalized Hermite function

$$h_n^{\gamma_j}(x) = e^{-x^2/2\gamma_j^2} H_n(x/\gamma_j)/\sqrt{\gamma_j \pi^{1/2} 2^n n!} \quad (20)$$

expressed in terms of the nth Hermite polynomial $H_n(x)$ [22].

The intermediate spectral state of photon 3 defined by Eq. (8) may be calculated analytically for the case of the Gaussian joint spectral amplitude in Eq. (16) and an initial spectral state for photon 1 defined by the complex-valued Gaussian amplitude

$$\alpha(\omega) = \left(\pi\sigma_1^2\right)^{-1/4}\exp\left[-\frac{(\omega-\bar\omega_1)^2}{2\sigma_1^2} + i\phi_1(\omega-\bar\omega_1) + i\frac{\phi_2}{2}(\omega-\bar\omega_1)^2\right]. \quad (21)$$

In Eq. (21), the real-valued parameters ϕ_1 and ϕ_2 represent the temporal delay and linear chirp rate, respectively, while σ_1 determines the spectral bandwidth. States of the form (21) may be generated experimentally, for example, using the techniques of Ref. [23]. Substituting Eqs. (16) and (21) into Eq. (8) yields an intermediate spectral state with the Gaussian form

$$|\tilde\psi_3\rangle = \eta \int d\omega \exp\left[-Q(\omega-\bar\omega_3)^2 + L(\omega-\bar\omega_3)\right]|\omega_3\rangle, \quad (22)$$

expressed in terms of the normalization constant

$$\eta = (2Q_R/\pi)^{1/4}\exp\left[-L_R^2/4Q_R - i\Phi_I\right], \quad (23)$$

the constant phase

$$\Phi_I = \frac{1}{2}\tan^{-1}[q/p] + \frac{pw-qs}{2(p^2+q^2)}, \quad (24)$$

the complex-valued quadratic coefficient

$$Q = Q_R - iQ_I, \quad (25)$$

with real component

$$Q_R = \frac{pr+q^2}{2\gamma_3^2(p^2+q^2)} \quad (26)$$

and imaginary component

$$Q_I = \frac{\rho^2\sigma_1^2 q}{2\gamma_3^2(p^2+q^2)}, \tag{27}$$

and the complex-valued linear coefficient

$$L = L_R - iL_I, \tag{28}$$

with real component

$$L_R = \rho\frac{\sigma_2(\delta p + qt)}{\sigma_3(p^2+q^2)} \tag{29}$$

and an imaginary component

$$L_I = L_I' + L_I'', \tag{30}$$

composed of a term proportional to ϕ_1,

$$L_I' = \frac{\rho\sigma_1^2\sigma_2 p}{\sigma_3(p^2+q^2)}\phi_1, \tag{31}$$

and a term proportional to ϕ_2,

$$L_I'' = \frac{\delta\rho\sigma_1^4\sigma_2}{\sigma_3(p^2+q^2)}\phi_2. \tag{32}$$

These latter quantities are expressed in terms of the definitions

$$\gamma_j^2 = \sigma_j^2(1-\rho^2), \tag{33}$$
$$\delta = \Omega - \bar{\omega}_1 - \bar{\omega}_2, \tag{34}$$
$$p = \sigma_1^2 + \gamma_2^2, \tag{35}$$
$$q = \gamma_2^2\sigma_1^2\phi_2, \tag{36}$$
$$r = \gamma_1^2 + \gamma_2^2, \tag{37}$$
$$s = \delta^2 + \sigma_1^2\gamma_2^2\phi_1, \tag{38}$$
$$t = \sigma_1^2(\delta\phi_2 + \phi_1), \tag{39}$$

and

$$w = \delta^2\sigma_1^2(\phi_2 + 2\phi_1), \tag{40}$$

with Ω the observed frequency of photon 4.

As an example, consider the case of a real-valued, transform-limited amplitude obtained by setting $\phi_1 = 0$ and $\phi_2 = 0$ in Eq. (21), for which Eq. (22) yields

$$|\tilde{\psi}_3\rangle = \left(\frac{r}{\pi\gamma_3^2 p}\right)^{1/4}\int d\omega \exp[-Q_R(\omega-\varepsilon)^2]|\omega_3\rangle, \tag{41}$$

where the spectral mean

$$\varepsilon = \bar{\omega}_3 - \delta\rho\frac{\sigma_2\sigma_3}{(\sigma_1^2+\sigma_2^2)} \tag{42}$$

depends on the spectral entanglement via ρ, the marginal bandwidths of all three photons, and the measurement outcome Ω via δ [cf. Eq. (34)]. When the bandwidths of photons 2 and 3 are identical, Eq. (42) may also be written as

$$\varepsilon = \bar{\omega}_3 - \frac{\delta\rho}{(a^2+1)}, \tag{43}$$

where $a = \sigma_1/\sigma_2$ is the bandwidth ratio of photon 1 to photon 2. Similarly, the quadratic coefficient in the exponent of (41) becomes

$$Q_R = \frac{a^2(a^2+1)}{2\sigma_1^2(a^2+1-\rho^2)}. \tag{44}$$

Hence, in the limit $|\rho|$ approaches unity and a approaches zero, the form of the spectral amplitude $\alpha(\omega)$ is recovered exactly, and the corresponding spectral shift $\Delta = \bar{\omega}_1 - \varepsilon$ reduces to the idealized result following Eq. (12). As discussed in detail later, unit fidelity is recovered whenever $a^4 = 1 - \rho^2$ (cf. the analysis of Fig. 3).

The spectral teleportation fidelity for the Gaussian input state of Eq. (21) is calculated using the definition of Eq. (14), with the teleported state given by Eq. (13). The latter is derived from the intermediate state given by Eq. (22) and the soon-to-be-determined spectral shift Δ. From this calculation, the spectral fidelity for a generic Gaussian amplitude is presented as

$$F = \left(\frac{2Q_R}{\sigma_1^2|Q+C|^2}\right)^{1/2}\exp[\Gamma(\tilde{\Delta})], \tag{45}$$

where the complex constant $C = (1+i\phi_2\sigma_1^2)/2\sigma_1^2$, the intermediate spectral shift $\tilde{\Delta} = \Delta + \bar{\omega}_3 - \bar{\omega}_1$, and the exponent

$$\Gamma(\tilde{\Delta}) = \mathrm{Re}\left\{\frac{(2Q\tilde{\Delta} + L - i\phi_1)^2}{2(Q+C)} - \frac{(2Q_R\tilde{\Delta} + L_R)^2}{2Q_R}\right\} \tag{46}$$

are introduced for notational convenience. The spectral shift that maximizes the teleportation fidelity is determined by differentiating Eq. (46) with respect to $\tilde{\Delta}$ and solving for the root to identify the optimal spectral shift Δ_{opt}. For example, when $\phi_1 = 0$ and $\phi_2 = 0$, maximization of the fidelity leads to the condition

$$\Delta_{\mathrm{opt}} = \bar{\omega}_1 - \bar{\omega}_3 - L_R/2Q_R, \tag{47}$$

which agrees with the result of Eq. (42). More generally, the spectral shift that maximizes the fidelity is given by

$$\Delta_{\mathrm{opt}} = \bar{\omega}_1 - \bar{\omega}_3 - \frac{(L_R C_R + L_I Q_I + \phi_1 Q_I)}{2(Q_I^2 + Q_R C_R)}, \tag{48}$$

with C_R the real component of C. A plot of Δ_{opt} with respect to a and ρ is shown in Fig. 1 for $\bar{\omega}_1 = \bar{\omega}_3$, $\phi_1 = 0$, $\phi_2 = 2/\sigma_1^2$, and $\delta = \sigma_1$. These results suggest that in the regime of large spectral entanglement (large $|\rho|$) the shift Δ_{opt} varies slowly with respect to a.

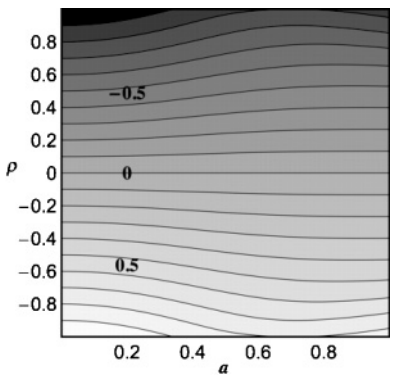

FIG. 1. A contour plot of the optimal spectral shift Δ_{opt} defined by Eq. (48) for a chirped input state. Contours are plotted with respect to the bandwidth ratio a and the linear correlation ρ with $\bar{\omega}_1 = \bar{\omega}_3$, $\phi_1 = 0$, $\phi_2 = 2/\sigma_1^2$, $\delta = \sigma_1$, and $\sigma_2 = \sigma_3$. Contours range from $-\sigma_1$ to σ_1 in intervals of $0.1\sigma_1$ with the line at $\rho = 0$ corresponding to $\Delta_{\mathrm{opt}} = 0$.

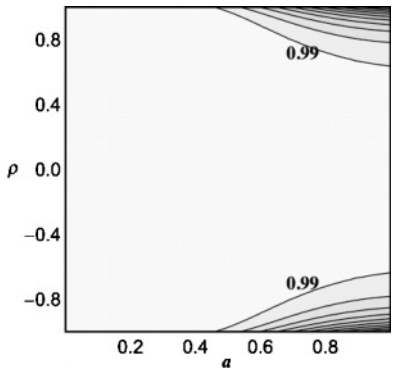

FIG. 2. A contour plot of $\exp[\Gamma(\tilde{\Delta}_{\text{opt}})]$ from Eq. (45) for a chirped input state. Contours are plotted with respect to the bandwidth ratio a and the linear correlation ρ with $\bar{\omega}_1 = \bar{\omega}_3$, $\phi_1 = 0$, $\phi_2 = 2/\sigma_1^2$, $\delta = \sigma_1$, and $\sigma_2 = \sigma_3$. Contours are unitless and range from 0.9 to 1 in intervals of 0.01 with the large centered region representing values equal to and above 0.99.

Application of the optimal spectral shift Δ_{opt} does not guarantee the exponent defined by Eq. (46) vanishes, only that it reaches the smallest possible value. The behavior for the exponential term on the right-hand side (RHS) of Eq. (45) evaluated at Δ_{opt} is shown with respect to a and ρ in Fig. 2 for the same parameters as in Fig. 1. Notably, this factor is near unity over a broad region of the a-ρ parameter space.

For a transform-limited input amplitude with $\phi_1 = 0$ and $\phi_2 = 0$, the exponent $\Gamma(\Delta_{\text{opt}})$ vanishes for all measurement outcomes and the fidelity in Eq. (45) is conveniently expressed in terms of the dimensionless quantities a and ρ as

$$F = \sqrt{\frac{4\kappa^2 a^2 (a^2+1)(a^2+1-\rho^2)}{[(a^2+\kappa^2)(a^2+1)-\kappa^2\rho^2]^2}}, \tag{49}$$

where the bandwidth ratio $\kappa = \sigma_3/\sigma_2$ need not be unity.

The behavior of the spectral fidelity for $\kappa = 1$ is plotted in Fig. 3 with respect to the bandwidth ratio a and the spectral correlation ρ. The four corners in this contour plot exhibit four limiting behaviors of spectral teleportation. In the lower right-hand corner, where $a = 1$ and $\rho = 0$, the bandwidths of all three photons are identical and there is necessarily perfect overlap between the initial state of photon 1 and the final state of photon 3. In the lower left-hand corner, where $a = 0$ and $\rho = 0$, the fidelity vanishes as this point corresponds to infinite bandwidths for photons 2 and 3 but no spectral entanglement and, consequently, an absence of teleportation. The upper left-hand corner, where $a = 0$ and $\rho = 1$, corresponds to the case of infinite spectral entanglement and infinite bandwidth for photons 2 and 3, the fidelity at this point is unity [cf. the example of Eq. (11)].

The upper right-hand corner of Fig. 3, where $a = 1$ and $\rho = 1$, represents a counterintuitive case for the spectral fidelity. Naively, unit fidelity is expected whenever $a = 1$, as the initial state of photon 1 matches the initial state of photon 3. However, the spectral measurement following up-conversion undermines this assumption because the measurement of photon 4 yields some information about the spectral states of photons 1 and 2. This is similar to the situation that occurs when the bandwidth of photon 2 is much less than the bandwidth of photon 1, that is, for $a > 1$, as then up-conversion acts as spectral gating of photon 1 with the measured frequency Ω providing information about the spectral state. In general, for $a = 1$ the measurement provides more information as $|\rho|$ approaches unity, that is, when photons 2 and 3 are perfectly entangled. In particular, the fidelity at the upper left-hand corner is $\sqrt{8/9}$, a value for the fidelity that corresponds to a state of photon 3 with half the initial bandwidth of photon 1 [cf. Eq. (44)]. The contour defined by $a^4 = 1 - \rho^2$ identifies maximization of the fidelity and represents the optimal compromise between spectral bandwidth and spectral entanglement.

A contour plot of the spectral teleportation fidelity for a linearly chirped input state is shown in Fig. 4 with $\phi_2 = 2/\sigma_1^2$. In contrast to the unchirped case, chirp in the input amplitude causes the fidelity at the point $a = 1$ and $\rho = 0$ to be less than unity as the unmodified state of photon 3 is unchirped. However, for $a < 1$ and ρ close to unity the fidelity approaches unity.

The behavior of the spectral teleportation fidelity with respect to the Schmidt number K is shown in Fig. 5. Using Eqs. (18) and (19), the fidelity from Eq. (45) is plotted against

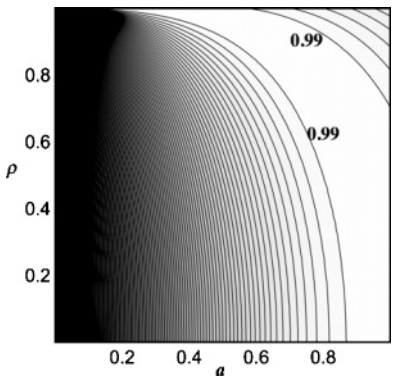

FIG. 3. A contour plot of the spectral teleportation fidelity F in Eq. (49) for an unchirped input state. Contours are plotted with respect to the bandwidth ratio a and the linear correlation ρ with $\bar{\omega}_1 = \bar{\omega}_3$, $\phi_1 = 0, \phi_2 = 0, \delta = \sigma_1$, and $\sigma_2 = \sigma_3$. Contours are unitless and range from 0 to 0.99 with a spacing of 1/50.

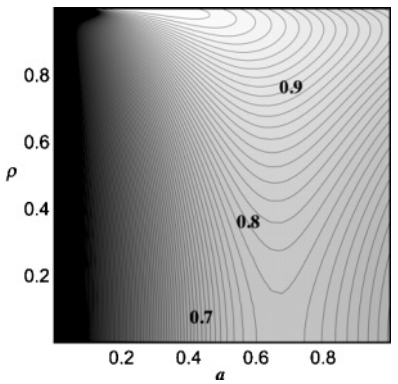

FIG. 4. A contour plot of the spectral teleportation fidelity F in Eq. (45) for a chirped input state. Contours are plotted with respect to the bandwidth ratio a and the linear correlation ρ with $\bar{\omega}_1 = \bar{\omega}_3$, $\phi_1 = 0$, $\phi_2 = 2/\sigma_1^2$, $\delta = \sigma_1$, and $\sigma_2 = \sigma_3$. Contours are unitless and range from 0 to 0.99 with a spacing of 1/50.

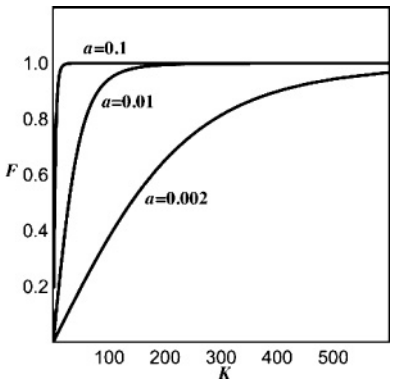

FIG. 5. A plot of the spectral teleportation fidelity in Eq. (45) for a chirped input state. Lines are plotted with respect to the spectral Schmidt number K with $\bar{\omega}_1 = \bar{\omega}_3$, $\phi_1 = 0$, $\phi_2 = 2/\sigma_1^2$, $\delta = \sigma_1$, and $\sigma_2 = \sigma_3$. Curves are labeled by the bandwidth ratio a: 1/10, 1/100, and 1/500. The point $K = 600$ corresponds to a spectral correlation of $\rho \cong 0.999999$.

K for $\sigma_2 = \sigma_3$ with each curve parametrized by the bandwidth ratio a. In addition, parameters for these curves are $\bar{\omega}_1 = \bar{\omega}_3$, $\phi_1 = 0$, $\phi_2 = 2/\sigma_1^2$, $\delta = \sigma_1$, and $\Delta = \Delta_{\text{opt}}$. As expected from the results presented by Figs. 3 and 4, the spectral entanglement needed for constant fidelity teleportation increases in Fig. 5 as the bandwidth ratio a decreases. We note that current SPDC sources of spectrally entangled photons are capable of generating spectral Schmidt numbers on the order of 600 [18] and potentially much higher [19,20]. As the value of $K = 600$ corresponds to a spectral correlation $\rho \cong 0.999999$, it is apparent from Figs. 4 and 5 that current sources of spectrally entangled photon pairs provide sufficient entanglement for high-fidelity spectral teleportation.

These examples have been with respect to specific input states, for which the parameters σ_1 and ϕ_2 describing the Gaussian spectral amplitude are fixed. By fixing these parameters we have shown there exists an optimal value of the spectral shift Δ. However, in order to assess the fidelity of teleporting states selected from an ensemble of nonorthogonal spectral amplitudes (an important distinction of quantum teleportation from classical communication), we must evaluate the spectral teleportation fidelity with respect to the distribution of presumedly unknown input states.

For example, consider the spectral bandwidth of photon 1 to be uniformly sampled from a spectral range $[\sigma_{\text{min}}, \sigma_{\text{max}}]$, where σ_{min} and σ_{max} represent minimal and maximal values, respectively. The distinction from our previous examples is the applied spectral shift Δ is chosen without explicit knowledge of the value of σ_1. In the current example, we assume the range of σ_1 is known and choose a spectral shift corresponding to the average bandwidth, that is, $\Delta = \Delta_{\text{opt}}$ when $\sigma_{1,\text{avg}} = (\sigma_{\text{max}} + \sigma_{\text{min}})/2$. As shown in Fig. 6, spectral teleportation fidelity for the distribution of input states characterized by $\sigma_{\text{min}} = \sigma_1/2$ and $\sigma_{\text{max}} = 2\sigma_1$ remains high provided the spectral entanglement is large ($|\rho| = 0.9999$, thick black line). This particular distribution of input states has a minimal overlap of $\sim$0.47 between states with bandwidths σ_{min} and σ_{max}, and an average fidelity of $\langle F \rangle = 0.996 \pm 0.003$. Lesser values of entanglement fail to produce the same high fidelity across the distribution of input states, for example, $\langle F \rangle = 0.882 \pm 0.101$

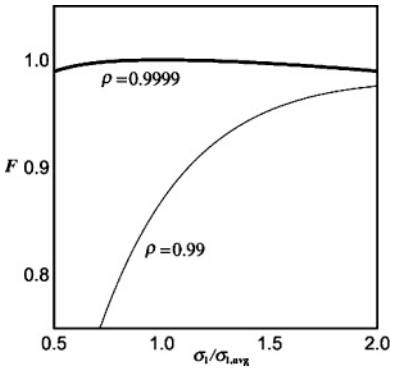

FIG. 6. A plot of the spectral teleportation fidelity with respect the bandwidth of the input Gaussian spectral state. The curves correspond to $\rho = 0.9999$ (thick) and $\rho = 0.99$ (thin) and are plotted against the bandwidth of photon 1 with respect to the average spectral bandwidth $\sigma_{1,\text{avg}}$. The applied spectral shift is referenced to $\sigma_{1,\text{avg}}$ and other parameters are $\sigma_2 = \sigma_3 = 10\sigma_{1,\text{avg}}$, $\phi_1 = 0$, $\phi_2 = 0$, and $\delta = \sigma_{1,\text{avg}}$ for degenerate mean frequencies.

for $|\rho| = 0.99$ (thin black line in Fig. 6). This decline in fidelity continues with decreasing entanglement until an average of $\langle F \rangle = 0.244 \pm 0.082$ is reached at $\rho = 0$.

A second example of different input states is given for the case of varying linear chirp rates ϕ_2, where the linear chirp rate is sampled from a uniform distribution over the range $[\phi_{2,\text{min}}, \phi_{2,\text{max}}]$ and has an average rate of $\phi_{2,\text{avg}} = (\phi_{2,\text{max}} + \phi_{2,\text{min}})/2$. The spectral teleportation fidelity is evaluated using the optimal spectral shift for the case of zero chirp and plotted in Fig. 7 as a function of the input chirp rate. For large spectral entanglement ($|\rho| = 0.9999$, thick black line) the average fidelity is $\langle F \rangle = 0.975 \pm 0.022$, while the average is $\langle F \rangle = 0.580 \pm 0.177$ for less spectral entanglement ($|\rho| = 0.99$, thin black line) and $\langle F \rangle = 0.104 \pm 0.047$ for no spectral entanglement ($|\rho| = 0$).

Last, we present in Fig. 8 the spectral teleportation fidelity for an ensemble of input states parametrized by both the bandwidth and the linear chirp rate, that is, (σ_1, ϕ_2). In this

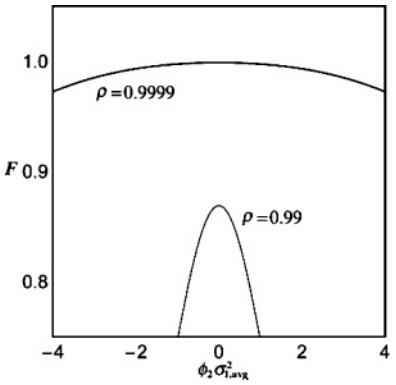

FIG. 7. A plot of the spectral teleportation fidelity with respect the linear chirp rate of the input Gaussian spectral state. The curves correspond to $\rho = 0.9999$ (thick) and $\rho = 0.99$ (thin) and are plotted against the chirp rate of photon 1 with respect to the average linear chirp rate $\phi_{2,\text{avg}}$. The applied spectral shift is referenced to $\phi_{2,\text{avg}} = 0$ and other parameters are $\sigma_2 = \sigma_3 = 10\sigma_1$, $\phi_1 = 0$, and $\delta = \sigma_1$ for degenerate mean frequencies.

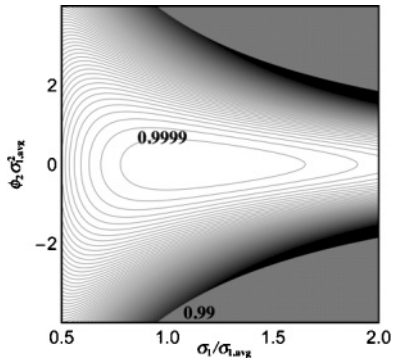

FIG. 8. A contour plot of the spectral teleportation fidelity with respect to the spectral bandwidth and linear chirp rate of the input Gaussian spectral state. Contours are plotted with respect to spectral bandwidth in terms of $\sigma_{1,\mathrm{avg}}$ and the linear chirp rate in terms of $\phi_{2,\mathrm{avg}}$ (cf. Figs. 6 and 7). The applied spectral shift is referenced to an unchirped state of bandwidth of $\sigma_{1,\mathrm{avg}}$ and other parameters are $\rho = 0.9999$, $\sigma_2 = \sigma_3 = 10\sigma_{1,\mathrm{avg}}$, $\phi_1 = 0$, and $\delta = 0.1\sigma_1$ for degenerate mean frequencies. Contours are unitless and range from 0.99 to 0.9999 in steps of 0.0001.

example, the applied spectral shift is optimal for the unchirped, nominal input state found at $(\sigma_1,\phi_2) = (\sigma_{1,\mathrm{avg}},0)$ and a measured frequency corresponding to $\delta = 0.1\sigma_{1,\mathrm{avg}}$. The average fidelity over the parameter space shown in Fig. 8 is $\langle F\rangle = 0.992 \pm 0.0127$ for $|\rho| = 0.9999$. As noted previously, current down-conversion sources can reach $|\rho| = 0.999999$, in which case the same ensemble of two-dimensional parametrized input states yields an average fidelity $\langle F\rangle = 0.9999 \pm 0.0001$. By comparison, the average fidelity is $\langle F\rangle = 0.097 \pm 0.060$ without entanglement ($|\rho| = 0$).

IV. SPREAD-SPECTRAL TELEPORTATION

In Secs. II and III, we described spectral teleportation for the faithful reproduction of a single-photon spectral amplitude. In this section, we describe how similar methods can be used to coherently dilate the spectral amplitude during the teleportation process. We refer to this process as spread-spectral teleportation because of the change in spectral bandwidth. As a clarifying example, consider the limit that the joint spectral amplitude takes the form

$$f(\omega,\omega') \to \delta(2\bar{\omega}_0 - \kappa\omega - \omega'), \tag{50}$$

where κ represents the orientation of the joint spectrum in the frequency space of photons 2 and 3; for example, recall $\kappa = \sigma_3/\sigma_2$ for the finite bandwidth Gaussian amplitude in Eq. (16). Joint amplitudes approximating the RHS of Eq. (50) with $\kappa \neq 1$ arise from broad-bandwidth pumping of type-II SPDC in long nonlinear crystals [24].[3] Inserting Eq. (50) into Eq. (8), the normalized intermediate state becomes

$$|\tilde{\psi}_3\rangle = \kappa^{-1/2}\int \alpha(\omega/\kappa)|(\omega - \Delta)_3\rangle d\omega. \tag{51}$$

[3]This behavior arises from the orientation of the phase-matching function $\Phi(\omega,\omega')$ in the birefringent medium relative to the pump pulse $A(\omega + \omega')$.

The result (51) represents a spectral state of photon 3 for which the spectral amplitude $\alpha(\omega)$ has been dilated by the factor κ and spectrally shifted by $\Delta = \kappa\Omega - 2\bar{\omega}_0$. The shift is defined in terms of the measured frequency Ω, as well as the properties of the entangled photon pair, that is, $2\bar{\omega}_0$ and κ, and can be applied as described previously (cf. Sec. II). Broadening ($\kappa > 1$) or narrowing ($\kappa < 1$) the spectral amplitude, however, requires coherently modulating the phase and amplitude of photon 3.

Dilation of the spectral amplitude in Eq. (51) transforms the quantum information in a photonic carrier of one bandwidth (photon 1) to a carrier of another bandwidth (photon 3). As spread-spectral teleportation preserves the amplitude-level information encoded in $\alpha(\omega)$, the dilation process complements existing proposals to spectrally shift quantum information from one frequency band to another, for example, from IR to visible. For example, dilation of the spectral amplitude enables quantum information transmitted by a broad-bandwidth photon to be transformed into a narrow-bandwidth photon that better resonates with (solid-state) transitions having narrow linewidths. Conversely, narrow-bandwidth quantum readout operations from solid-state devices can be coherently transformed into broad-bandwidth photons by spread-spectral teleportation, for example, to improve resolution in the time of arrival.

Assessment of the spread-spectral teleportation fidelity differs slightly from the fidelity for conventional teleportation, where the initial spectral state of photon 1 is overlapped with the state prepared by teleportation. For spread-spectral teleportation, a reference spread spectral state is defined,

$$|\psi_1(\mu)\rangle = \mu^{-1/2}\int \alpha(\omega/\mu)|(\omega - \varepsilon_\mu)_1\rangle d\omega, \tag{52}$$

where the constant μ represents the dilation factor and the spectral offset $\varepsilon_\mu = (1-\mu)\bar{\omega}_1$ maintains the spectral mean of $\alpha(\omega)$ as $\bar{\omega}_1$. Overlapping the state (52) with the state prepared by spread-spectral teleportation yields the spread-spectral teleportation fidelity defined with respect to μ as

$$F_\mu = |\langle\psi_1(\mu) \mid \psi_3\rangle|^2. \tag{53}$$

In Eq. (53), the spread-spectral state $|\psi_3\rangle$ is given by Eq. (13) and, based on prior arguments, the spread-spectral teleportation fidelity is expected to be maximal when the bandwidth ratio κ of the mediating photon pair matches the dilation factor μ. Note that for $\mu = 1$ the conventional spectral teleportation fidelity is recovered.

V. GAUSSIAN SPREAD-SPECTRAL TELEPORTATION

We investigate the spread-spectral teleportation fidelity F_μ defined by Eq. (53) for the dilation of a complex-valued Gaussian spectral amplitude. We calculate the spectral amplitude of Eq. (21) with the joint spectral amplitude of Eq. (16), whose bandwidth ratio is $\kappa = \sigma_3/\sigma_2$. The spread-spectral teleportation fidelity defined in Eq. (53) is then given by

$$F_\mu = \left(\frac{2\mu^2 Q_R}{\sigma_1^2|\mu^2 Q + C|^2}\right)^{1/2}\exp\left[\Gamma_\mu(\tilde{\Delta})\right], \tag{54}$$

where $\tilde{\Delta} = \Delta + \bar{\omega}_3 - \bar{\omega}_1$ and

$$\Gamma_\mu(\tilde{\Delta}) = \mathrm{Re}\left\{ \frac{(2Q\mu\tilde{\Delta} + \mu L - i\phi_1)^2}{2(\mu^2 Q + C)} - \frac{(2Q_R\tilde{\Delta} + L_R)^2}{2Q_R} \right\}, \tag{55}$$

while other quantities remain as defined in Eqs. (22)–(40). The optimal spectral shift of photon 3 is found by differentiating Eq. (55) and finding the root that maximizes the exponential term on the RHS of Eq. (54). This approach yields

$$\Delta_{\mathrm{opt}} = \bar{\omega}_1 - \bar{\omega}_3 - \frac{(\mu^2 Q_I L_I + L_R C_R + \mu\phi_1 Q_R)}{2\left(\mu^2 Q_I^2 + Q_R C_R\right)}, \tag{56}$$

which reduces to Eq. (48) when $\mu = 1$.

When $\phi_1 = 0$ and $\phi_2 = 0$, the exponent $\Gamma_\mu(\Delta_{\mathrm{opt}})$ vanishes for all values of δ and μ, and the spread-spectral teleportation fidelity (54) reduces to

$$F_\mu = \sqrt{\frac{4\kappa^2\mu^2 a^2(a^2+1)(a^2+1-\rho^2)}{[(a^2+1)(\mu^2 a^2 + \kappa^2) - \kappa^2\rho^2]^2}}, \tag{57}$$

which differs slightly from the spectral teleportation presented in Eq. (49) due to the inclusion of the dilation factor μ. However, the behaviors of the spectral and spread-spectral teleportation fidelities are identical when $\mu = \kappa$, and Figs. 3 and 4 thus represent the spread-spectral teleportation fidelity for all values of $\kappa = \mu$. This result implies that *there is no inherent loss in fidelity due to dilation of the spectral state*.

A comparison of the spread-spectral teleportation fidelity for various values of κ is presented in Fig. 9. The dilation factor $\mu = 2$ is fixed and the fidelity is plotted with respect to the Schmidt number K for $\kappa = 2$, 4, and 8. Results for chirped (solid lines) and unchirped (dashed lines) input states are presented. For these curves, the values $a = 0.1$, $\delta = \sigma_1$, $\phi_1 = 0$, and $\phi_2 = 2/\sigma_1^2$ are fixed. For $\kappa \neq \mu$, the fidelity is low even for large K and, while unseen in Fig. 9, those inferior fidelities do not approach unity in the limit K approaches infinity.

The state prepared by spread-spectral teleportation is defined by Eq. (13), and, for the case of Gaussian inputs, is derived from the intermediate state of Eq. (22) by applying

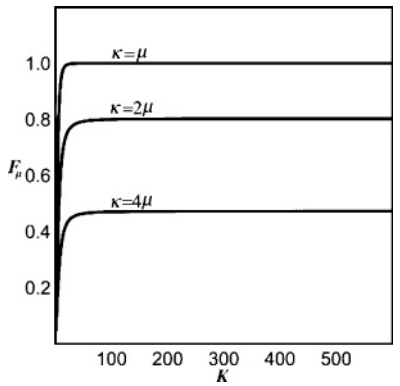

FIG. 9. A plot of the spread-spectral teleportation fidelity F_μ for different bandwidth ratios κ. Lines are plotted with respect to the spectral Schmidt number K with $\mu = 2$, $a = 0.1$, $\bar{\omega}_1 = \bar{\omega}_3$, $\phi_1 = 0$, $\phi_2 = 2/\sigma_1^2$, and $\delta = \sigma_1$. Curves are labeled by the bandwidth ratio κ relative to the dilation factor μ.

the optimal spectral shift defined by Eq. (56). In Fig. 10, the teleported spectral amplitude $\langle\omega \mid \psi_3\rangle$ is plotted with respect to ω for fixed values of the spectral correlation ρ. The panels in Fig. 10 show the change in form of the teleported state as the degree of spectral entanglement (indicated by either K or $|\rho|$) increases. In Fig. 10, the values $a = 0.1$, $\phi_1 = 0$, $\phi_2 = 2/\sigma_1^2$, $\delta = \sigma_1$, and $\mu = \kappa = 2$ are fixed. In panel (a), the amplitude (thick solid line) and phase (thick dashed line) of photon 3 is significantly different from the amplitude and phase of photon 1 (thin lines). As ρ approaches unity, indicated by the progression of panels (a) through (d), the amplitude and phase of the teleported state approach that of the intended spread-spectral state.

As with spectral teleportation, the spread-spectral teleportation fidelity is averaged with respect to the distribution of possible input states. As noted earlier, there is no inherent loss to the fidelity of teleportation from spreading the spectrum when the bandwidth ratio κ matches the spreading factor μ. Consequently, the averages computed in Sec. III with respect to distributions of the input spectral state are also representative of the average fidelities expected from spread-spectral teleportation.

VI. DISCUSSION

As with previous variants of quantum teleportation, spectral teleportation suggests an opportunity to extend the transmission range of spectrally encoded quantum information; for example, by enabling a quantum repeater or quantum relay for long-distance, spectrally encoded quantum communication over noisy channels. In addition, spectral teleportation complements existing schemes to teleport the polarization [5,6] and transverse-spatial [7] degrees of freedom. When combined, these protocols enable a single platform for teleporting the multiple photonic degrees freedom, including the complete single-photon state [25–27], and, thus, greatly expand the size of the photonic Hilbert space accessible for encoding and processing quantum information.

Spread-spectral teleportation shows a similar promise supplemented by the ability to modulate broad-bandwidth photonic carriers for interacting with narrowband quantum receivers. For example, whereas broad bandwidths are favorable for ensuring timely transmission, absorption by atomic vapor atoms, neutral atoms, or trapped ions favors photons of narrower bandwidths. This capability may prove useful in long-distance quantum networks, where nodes composed from solid-state quantum memories require a teleportation-based protocol for communication. In addition, the capability to spread the spectral state of the photon enables a quantum variant of classical spread spectrum communication techniques. The analogy arises from both the broadening of the spectral bandwidth and the randomized spectral shifting induced by the measurement process [28].

The most significant technical challenge associated with the current formulation of spectral and spread-spectral teleportation is the use of biphoton up-conversion as the operation to entangle photons 1 and 2. Because the second-order nonlinearity associated with SFG is generally on the order of 10^{-12} m/V, the conversion efficiency for the proposed entangling operation is small. However, we note that parametric single-photon

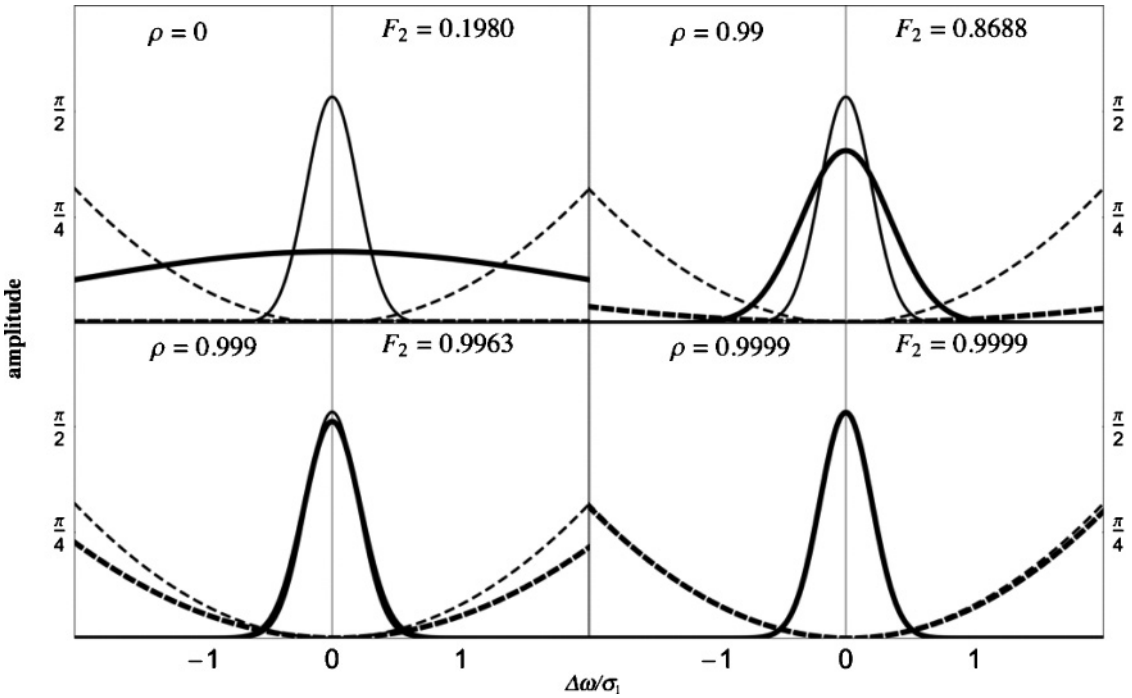

FIG. 10. Plots of the initial and teleported spectral amplitude at four values of ρ. Curves represent the magnitude (thin solid line) and phase (thin dashed line) of the initial wave form and the magnitude (thick solid line) and phase (thick dashed line) of the spread-spectral state. Plots are made with $\bar{\omega}_1 = \bar{\omega}_3$, $a = 0.1$, $\phi_1 = 0$, $\phi_2 = 2/\sigma_1^2$, $\delta = \sigma_1$, and $\mu = \kappa = 2$. The spectral shift Δ_{opt} from Eq. (56) has been applied and the difference frequency $\Delta\omega = \omega - \bar{\omega}_1$ is presented in units of σ_1. Panels correspond to values of the spectral correlation ρ: (a) 0, (b) 0.99, (c) 0.999, and (d) 0.9999; and yield the corresponding spread-spectral fidelities F_μ: (a) 0.1980, (b) 0.8688, (c) 0.9963, and (d) 0.9999.

frequency up-conversion has been successfully implemented, that is, assisted by a strong, coherent beam [11–14]. It may, therefore, be possible to implement the frequency-entangling operation required here using a similar form of parametric biphoton up-conversion, for example, four-wave mixing, assisted by a coherent beam, that could have a potential to occur with unit efficiency [29]. In that case, an open question is whether the spectral amplitude of the coherent field will affect the resulting teleported spectral state.

VII. CONCLUSIONS

We have presented a method for teleporting a single-photon spectral state using a spectrally entangled biphoton state. We have investigated the fidelity of spectral teleportation for the case of Gaussian spectral amplitudes, and we have described the behavior of the fidelity with respect to the relative bandwidths of the photons and the finite entanglement of the biphoton state. We have also shown how control over the marginal bandwidth ratio of the biphoton spectral amplitude permits arbitrary spreading of the spectral state prepared by teleportation. By investigating the spreading of complex Gaussian input states, we have shown that spread-spectral teleportation performs the same as spectral teleportation provided the appropriate definition of fidelity with respect to dilation is used. Based on estimates of spectral entanglement available from current SPDC-based photon pair sources, we conclude that spectral and spread-spectral teleportation fidelities as high as 0.9999 are obtainable with existing entanglement resources.

ACKNOWLEDGMENTS

This work has been sponsored by UT-Battelle, LLC, under Contract No. DE-AC05-00OR22725 with the US Department of Energy.

APPENDIX

For completeness, we present the relationships between the Gaussian parameters used in Eq. (16) and the experimental conditions determining the joint spectral amplitude of Eq. (15). Specifically, consider the SPDC phase-matching function of a bulk nonlinear crystal of length L to be

$$\Phi(\omega,\omega') = \text{sinc}[\Delta\mathbf{k}(\omega,\omega')\cdot\hat{\mathbf{z}}L/2], \tag{A1}$$

where $\text{sinc}[x] = \sin[x]/x$ and $\hat{\mathbf{z}}$ is perpendicular with the crystal face. The wave-vector phase mismatch $\Delta\mathbf{k}$ is

$$\Delta\mathbf{k}(\omega,\omega') = \mathbf{k}_p(\omega+\omega') - \mathbf{k}_o(\omega) - \mathbf{k}_e(\omega'), \tag{A2}$$

where indices o and e denote the ordinary and extraordinary down-converted rays, p denotes the pump pulse, and $\mathbf{k}_s$ is the wave vector for $s = p$, o, and e. By expanding the phase mismatch to first order in the difference frequencies $\omega - \omega_0$ and $\omega' - \omega_0$, and assuming down-conversion is matched at zeroth order, the phase matching function can be expressed as

$$\Phi(\omega,\omega') \cong \exp\{-\gamma[\tau_o(\omega-\omega_0) + \tau_e(\omega'-\omega_0)]^2\} \tag{A3}$$

with the constant $\gamma \cong 0.04823$ chosen to match the full width at half maximum (FWHM) of the Gaussian envelope to the FWHM of the phase-matching function. Under these conditions, the overlap between Eqs. (A1) and (A3) is ~0.94,

while within ± 1 FWHM the overlap is ~ 0.9999. Since spectral teleportation works best in a regime where the marginal bandwidths of the joint spectrum are much greater than the input spectral state, we anticipate the Gaussian approximation to be sufficient for modeling the teleported spectral state.

Using primes to denote derivatives, the time constants in Eq. (A3) are

$$\tau_o = L[k_p'(2\omega_0) - k_o'(\omega_0)] \tag{A4}$$

and

$$\tau_e = L[k_p'(2\omega_0) - k_e'(\omega_0)], \tag{A5}$$

which represent the differences in transit times through the crystal between the pump and o and e rays, respectively. Then, assuming the pump spectrum is a normalized Gaussian with the $1/e$ width σ_p, and using Eqs. (15) and (A3), we identify the Gaussian parameters in Eq. (16) as

$$\sigma_2^2 = \frac{1 + \gamma \tau_e^2 \sigma_p^2}{\gamma |\tau_o - \tau_e|^2}, \tag{A6}$$

$$\sigma_3^2 = \frac{1 + \gamma \tau_o^2 \sigma_p^2}{\gamma |\tau_o - \tau_e|^2}, \tag{A7}$$

and

$$\rho = \frac{-\left(1 + \gamma \tau_e \tau_o \sigma_p^2\right)}{\sqrt{\left(1 + \gamma \tau_o^2 \sigma_p^2\right)\left(1 + \gamma \tau_e^2 \sigma_p^2\right)}}. \tag{A8}$$

The linear correlation ρ can also be expressed simply in terms of the pump-pulse bandwidth σ_p and the marginal bandwidths σ_2 and σ_3 as [30]

$$\rho = \frac{2\sigma_p^2 - \left(\sigma_2^2 + \sigma_3^2\right)}{2\sigma_2 \sigma_3}. \tag{A9}$$

From the latter, it is obvious that there is no spectral entanglement when the signal and idler marginal bandwidths are equal to the pump bandwidth and that the maximal value for ρ occurs when $\sigma_2^2 = \sigma_3^2 = \sigma_p^2/2$. The minimal value of ρ occurs whenever σ_p is much smaller than the bandwidth of the down-converted photons; this condition implies phase-matching over a broad range of frequencies.

[1] C. H. Bennett, G. Brassard, C. Crepeau, R. Jozsa, A. Peres, and W. K. Wootters, Phys. Rev. Lett. **70**, 1895 (1993).
[2] S. L. Braunstein and H. J. Kimble, Phys. Rev. Lett. **80**, 869 (1998).
[3] T. Ide, H. F. Hofmann, T. Kobayashi, and A. Furusawa, Phys. Rev. A **65**, 012313 (2001).
[4] I. Marcikic *et al.*, Nature (London) **421**, 509 (2002).
[5] D. Bouwmeester *et al.*, Nature (London) **390**, 575 (1997).
[6] Y.-H. Kim, S. P. Kulik, and Y. Shih, Phys. Rev. Lett. **86**, 1370 (2001).
[7] S. P. Walborn, S. P. Walborn, D. S. Ether, R. L. deMatosFilho, and N. Zagury, Phys. Rev. A **76**, 033801 (2007).
[8] S. N. Molotkov, Phys. Lett. A **245**, 339 (1998).
[9] S. N. Molotkov and S. S. Nazin, Phys. Lett. A **252**, 1 (1999).
[10] W. P. Grice and I. A. Walmsley, Phys. Rev. A **56**, 1627 (1997).
[11] M. A. Albota and F. N. C. Wong, Opt. Lett. **29**, 1449 (2004).
[12] R. V. Roussev *et al.*, Opt. Lett. **29**, 1518 (2004).
[13] A. P. van Devender and P. G. Kwiat, J. Opt. Soc. Am. B **24**, 295 (2007).
[14] H. Takesue, Phys. Rev. Lett. **101**, 173901 (2008).
[15] S. Parker, S. Bose, and M. B. Plenio, Phys. Rev. A **61**, 032305 (2000).
[16] T. S. Humble and W. P. Grice, Phys. Rev. A **75**, 022307 (2007).
[17] T. S. Humble and W. P. Grice, Phys. Rev. A **77**, 022312 (2008).
[18] M. Avenhaus, M. V. Chekhova, L. A. Krivitsky, G. Leuchs, and C. Silberhorn, Phys. Rev. A **79**, 043836 (2009).
[19] Yu. M. Mikhailova, P. A. Volkov, and M. V. Fedorov, Phys. Rev. A **78**, 062327 (2008).
[20] G. Brida *et al.*, Europhys. Lett. **87**, 64003 (2009).
[21] W. Mauerer and C. Silberhorn, AIP Conf. Proc. **1110**, 220 (2009).
[22] P. M. Morse and H. Feshbach, *Methods of Theoretical Physics* (McGraw Hill, New York, 1953).
[23] X. Shi, A. Valencia, M. Hendrych, and J. P. Torres, Opt. Lett. **33**, 875 (2008).
[24] W. P. Grice, A. B. U'Ren, and I. A. Walmsley, Phys. Rev. A **64**, 063815 (2001).
[25] T. S. Humble, R. S. Bennink, and W. P. Grice, *Quantum Electronics and Laser Science Conference, OSA Technical Digest (CD)* (Optical Society of America, 2008), paper JTuA110.
[26] T. S. Humble, R. S. Bennink, and W. P. Grice, Proc. SPIE **7092**, 70920V (2008).
[27] D. S. Ether, S. P. Walborn, and N. Zagury, Phys. Rev. A **79**, 032305 (2009).
[28] T. S. Humble, *Quantum Electronics and Laser Science Conference, OSA Technical Digest (CD)* (Optical Society of America, 2010), paper QThI7.
[29] Z. Y. Ou, Phys. Rev. A **78**, 023819 (2008).
[30] W. P. Grice and T. S. Humble (unpublished).